

A Novel Robotic-Assisted Rehabilitation System for Elbow Fracture: Design and Full-Cycle Rehabilitation Strategy

Qianze Helian[®], Jiade Chang, Zhiyuan He[®], and Tao Sun[®], Senior Member, IEEE

Abstract -- Postoperative rehabilitation is critical for restoring elbow function following fractures, yet current approaches face significant limitations. Manual rehabilitation lacks precision and relies heavily on subjective experience, while existing robotic systems, primarily designed for neurological rehabilitation, fail to provide essential joint traction capabilities. In this paper, a novel robotic system integrating elbow rotation and traction functions (ERT-Robot) is proposed to provide full-cycle rehabilitation training. The system features an adaptive rotation mechanism that accommodates upper limb biomechanics and a traction mechanism for soft tissue stretching, ensuring wide patient applicability. A full-cycle rehabilitation protocol incorporating three therapeutic modalities: reciprocating passive training, active range of motion training, and muscle strength training, is introduced to address diverse clinical needs across all rehabilitation phases. Experimental validation involving six healthy subjects demonstrated that the robotic system significantly increased both horizontal and vertical olecranon displacements compared to natural arm rotation. Quantitative analysis showed minimal differences between manual and robot-assisted rehabilitation, with mean displacement variations of merely 1.33% (horizontal) and 7.78% (vertical), demonstrating clinically comparable performance. In addition, experimental results

Received 15 March 2025; revised 7 June 2025; accepted 10 June 2025. Date of publication 13 June 2025; date of current version 20 June 2025. This work was supported in part by China Postdoctoral Science Foundation under Grant 2024M752356, in part by the Postdoctoral Fellowship Program of China Postdoctoral Science Foundation (CPSF) under Grant GZC20231911, in part by the Key Project of Applied Basic Research in Tianjin under Grant 22JCZDJC00150 and Grant 22JCYBJC01670, in part by the Open Fund of Key Laboratory of Mechanism Theory and Equipment Design of Ministry of Education (Tianjin University), and in part by the Basic Public Welfare Research Project of Shaoxing under Grant 2024A14003. (Corresponding author: Zhiyuan He.)

This work involved human subjects or animals in its research. Approval of all ethical and experimental procedures and protocols was granted by the Ethics Committee of Tianjin University under Application No. TJUE-2024-549.

Qianze Helian and Jiade Chang are with the Key Laboratory of Mechanism Theory and Equipment Design of Ministry of Education, Tianjin University, Tianjin 300350, China (e-mail: helianqz@tju.edu.cn; jiadechang@tju.edu.cn).

Zhiyuan He and Tao Sun are with the Key Laboratory of Mechanism Theory and Equipment Design of Ministry of Education, Tianjin University, Tianjin 300350, China, and also with the International Institute for Innovative Design and Intelligent Manufacturing, Tianjin University, Shaoxing, Zhejiang 312077, China (e-mail: hezhiyuan@tju.edu.cn; stao@tju.edu.cn).

Digital Object Identifier 10.1109/TNSRE.2025.3579374

in three rehabilitation modalities confirmed the system's feasibility and efficiency for postoperative elbow fracture management.

Index Terms— Elbow fracture, postoperative rehabilitation robot, full-cycle rehabilitation, joint traction training, deep learning.

I. INTRODUCTION

C LOBAL fracture incidence exceeds 178 million cases annually, with elbow fractures accounting for over 12 million cases [1], creating substantial demand for rehabilitation services. The elbow joint, facilitating more than 60% of hand movements and involving 15 upper limb skeletal muscles, presents complex rehabilitation challenges with prolonged recovery periods. Inadequate postoperative rehabilitation often leads to severe complications, including muscle atrophy, periarticular tissues adhesion, and joint stiffness [2], [3]. Consequently, elbow fracture rehabilitation has emerged as a critical focus in orthopedic medicine.

Existing elbow fracture rehabilitation methods, including both manual therapy and robot-assisted approaches, present significant clinical limitations. While manual rehabilitation has proven effective in reducing postoperative complications [4], its heavy reliance on clinicians' subjective experience leads to inconsistent treatment precision and compromised outcome stability. Although existing rehabilitation robots have represented technological progress, most designs overlook the critical requirement for controlled joint traction. This fundamental deficiency ultimately impairs their ability to ensure precise traction control, which is a key determinant of both efficacy and safety in elbow fracture rehabilitation.

Currently, the majority of fracture rehabilitation research is primarily focused on the lower limb joints, such as the hip joint [5], knee joint [6], and ankle joint [7]. These studies mainly revolve around aspects like weight-bearing, axial loading, and rehabilitation methods. Through clinical trials and experimental research, researchers have validated the rehabilitation effects of exoskeletons and other rehabilitation devices on patients with lower limb fractures after surgery. However, in contrast to the lower limb joints, there is currently a lack of robotic systems specifically designed for the rehabilitation of elbow fractures. Existing elbow rehabilitation robots

predominantly adopt either serial or parallel configurations, primarily designed for neurorehabilitation. These systems typically feature single degree of freedom (DoF) rotational movement. Early developments include CADEN-7, a serial rigid robot proposed by Perry et al. [5], [8], which achieved comprehensive upper limb motion but suffered from excessive bulk. Chen et al. [9] developed a parallel exoskeleton employing cable-driven differential mechanisms for forearm rotation, with limited joint mobility. Irshaidat et al. [10] introduced a lightweight parallel pneumatic system for elbow rehabilitation, offering enhanced portability and safety. However, these systems share critical limitations: inability to perform elbow traction and adapt to individual carrying angles, rendering them unsuitable for fracture rehabilitation. The elbow's complex biomechanics involve coupled flexion-extension with rotational and sliding motions. Isolated rotational movement without sliding deviates from natural joint kinematics, potentially causing secondary fractures. While immobilization remains the standard therapeutic approach for elbow trauma, prolonged braking induces tissue stress deprivation, leading to ligament/tendon contracture, muscle atrophy, and joint stiffness [11]. Consequently, controlled joint traction is crucial for effective rehabilitation. Furthermore, robotic systems must accommodate individual carrying angle variations, as improper fixation may result in secondary injuries. Based on these considerations, the JAS company proposed an elbow rehabilitation orthosis that incorporates traction training functionality [12], [13]. However, its manual adjustment mechanism lacks electronic control, resulting in imprecise movement and absence of carrying angle adaptation. And the system offers only two predefined rehabilitation trajectories, lacking both customized training protocols and active rehabilitation capabilities, significantly limiting its effectiveness in muscle strength recovery.

In addition to the mechanical structure of robots, control strategies are another important factor affecting rehabilitation outcomes. Based on patient involvement, existing control strategies can be classified into passive and active modes. Passive control, employing trajectory tracking methods such as proportional-integral-derivative (PID) [14], back-stepping [15], time-lag [16], and sliding mode control [17], is primarily applied in early rehabilitation phases for patients with limited mobility. However, studies show that exclusive reliance on passive training has a suboptimal outcome [18], [19]. Active control strategies are suitable for mid-to-late phase patients with partial mobility. Elbow exoskeleton NEU-ROExos [20] implemented variable impedance actuation, offering independent and near-zero impedance torque control. AGREE robot [21] employed impedance control with three human-robot interaction modes. Unfortunately, existing studies on passive and active control have neglected joint traction implementation.

In recent years, motion estimation represents a critical advancement in active control strategies, since it has foresight for the generation of force and motion. Physiological signals, such as surface electromyographic (sEMG), was one of the most common methods for motion estimation. This method could reduce human-robot interaction forces, making it particularly suitable for postoperative fracture rehabilitation

[22]. Wu et al. [23] developed a hybrid model integrating sEMG-based elbow joint motion estimation with neural network compensation and adaptive control, enhancing patient engagement and training safety. Gui et al. [24] introduced a radial basis function neural network approach for sEMG-based motion estimation, eliminating myoelectric-moment model calibration. However, these studies focus on the estimation of joint motion angles, lack of traction prediction capabilities, and are not applicable to fracture rehabilitation needs.

In summary, current research on elbow rehabilitation robots critically overlooks joint traction function, potentially leading to postoperative complications or secondary fractures, while lacking appropriate control strategies for fracture rehabilitation. To address these issues, a novel robotic system integrating elbow rotation and traction functions (ERT-Robot) is proposed to provide full-cycle rehabilitation training. The system features adaptive mechanisms accommodating individual variations in carrying angle, arm length, and circumference. A full-cycle rehabilitation control method is developed for comprehensive rehabilitation across all phases through joint traction regulation. The early-phase protocol employs a position-force controller to replicate natural 2-DOF elbow motion. For mid-phase rehabilitation, a Convolutional Neural Network-Long Short-Term Memory-Attention (CNN-LSTM-Attention) model for sEMG-based estimation of rotation angles and traction forces is designed. The late-phase protocol incorporates an admittance control model simulating muscle loading, enabling personalized rehabilitation training. The efficiency of proposed method was validated through the experiments with six healthy subjects.

The rest of this paper is organized as follows. Section II presents the design of ERT-Robot. Section III introduces the control method for full-cycle rehabilitation. Experimental results and discussions are presented in Section VI and Section V. Finally, Section VI concludes this article.

II. ROBOT DESIGN

The structural configuration of the proposed ERT-Robot, comprising two primary components: an upper arm exoskeleton and a forearm exoskeleton, interconnected through a carrying angle mechanism, as shown in Fig. 1. The forearm exoskeleton integrates a traction mechanism (Fig. 1 (c)) and fixation structure, while the upper arm exoskeleton contains its corresponding fixation assembly. The robot provides -5° to 145° rotation and $\pm 15^{\circ}$ swing, encompassing the natural range of elbow joint motion [3]. With a total mass of 3.74 kg (without DC power supply), the ERT-Robot demonstrates compact and lightweight design characteristics.

A. Joint Traction Function

The proposed traction mechanism enables simultaneous joint rotation and traction through a U-shaped slider integrated with the forearm exoskeleton, as shown in Fig. 2.

This configuration features U-shaped slider mounted on bilateral rails, securely attached to the patient's forearm. Each side incorporates an electric cylinder connected to the slider base via revolute joint, providing linear actuation. During

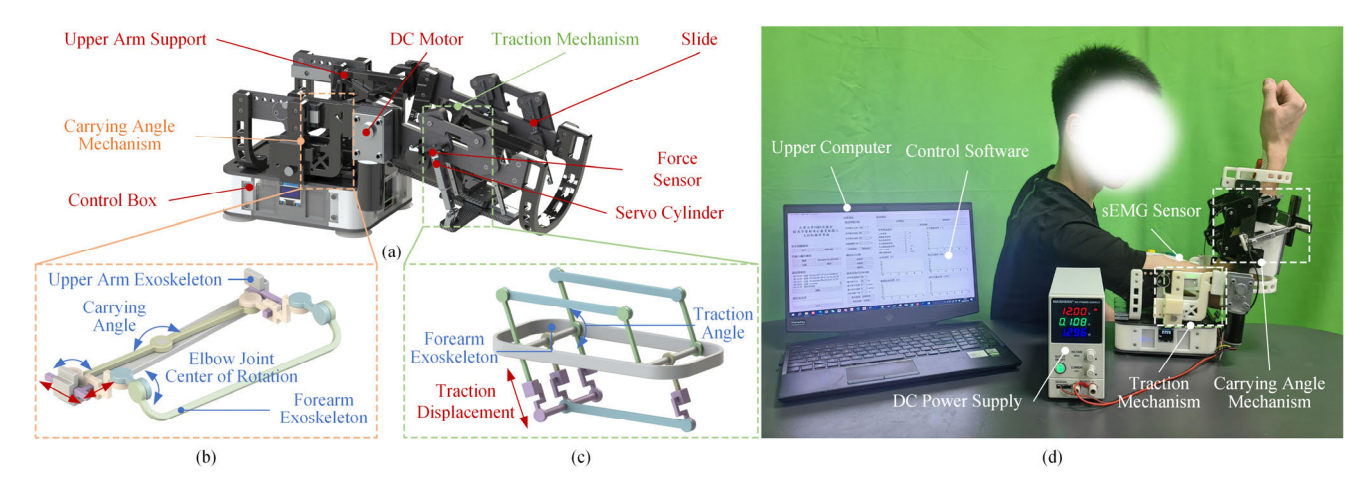


Fig. 1. ERT-Robot system overview. (a) Virtual prototype, (b) Carrying angle mechanism, (c) Traction mechanism, and (d) Physical prototype.



Fig. 2. Structural configuration of ERT-Robot traction mechanism.

operation, the cylinders drive the sliders to move along the rails, generating controlled traction. The system achieves 0-16 mm displacement with a maximum traction force of 70 N.

To enable personalized rehabilitation, the traction force direction relative to the forearm axis is made adjustable through a dual-parallelogram mechanism. Two parallel sliding rails on each side maintain U-shaped slider alignment with the forearm exoskeleton. The mounting brackets of electric cylinder, connected to the forearm exoskeleton the via revolute joint, incorporate internal nut slides for manual tightening. This design enables wide-angle adjustment: tightening the two hand screws locks the traction angle in place, while loosening them allows for orientation adjustment of both the cylinders and rails. The mechanism provides adjustable traction angles ranging from 45° to 85°.

B. Adjustment Function

The carrying angle, defined as the acute angle between the upper arm and forearm axes, averages 12.88°±5.92° in

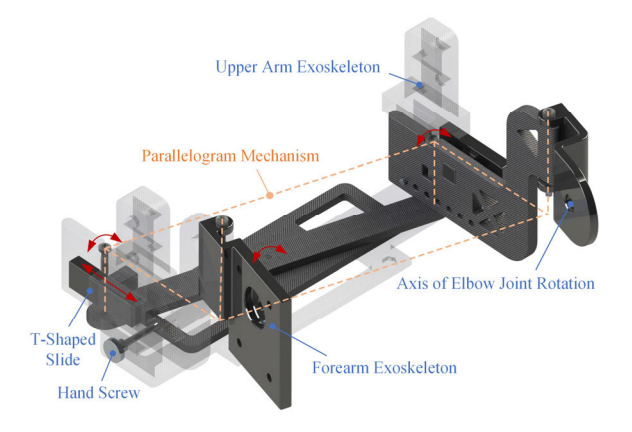


Fig. 3. Structural configuration of ERT-Robot carrying angle mechanism.

adults (males: $10.97^{\circ}\pm4.27^{\circ}$, females: $15.07^{\circ}\pm4.95^{\circ}$) [25]. To accommodate individual variations, an adaptive carrying angle mechanism based on a parallelogram configuration is developed, as shown in Fig. 3. The mechanism features a parallelogram structure with a bearing at the midpoint of one long side, connecting to the upper arm exoskeleton. T-shaped sliders on both sides have horizontal parts sliding within the upper arm exoskeleton and vertical parts sliding within a connecting piece. This piece links to the forearm exoskeleton via a revolute joint equipped with a DC motor for elbow rotation. When the parallelogram's long side rotates, the sliders and connecting pieces move in sequence, causing the forearm exoskeleton to swing, adjusting the carrying angle from -15° to 15° .

To ensure human-robot compatibility, the system incorporates adjustable dimensions accommodating upper limb anthropometric variations. Based on Chinese national standards for body dimensions [26], the design addresses four key parameters: upper arm length, upper arm circumference, forearm length, and forearm circumference. The upper arm exoskeleton features a sliding rail mechanism with U-shaped fixation brackets, allowing six-position length adjustment at 15 mm intervals via pins. For circumference adaptation,

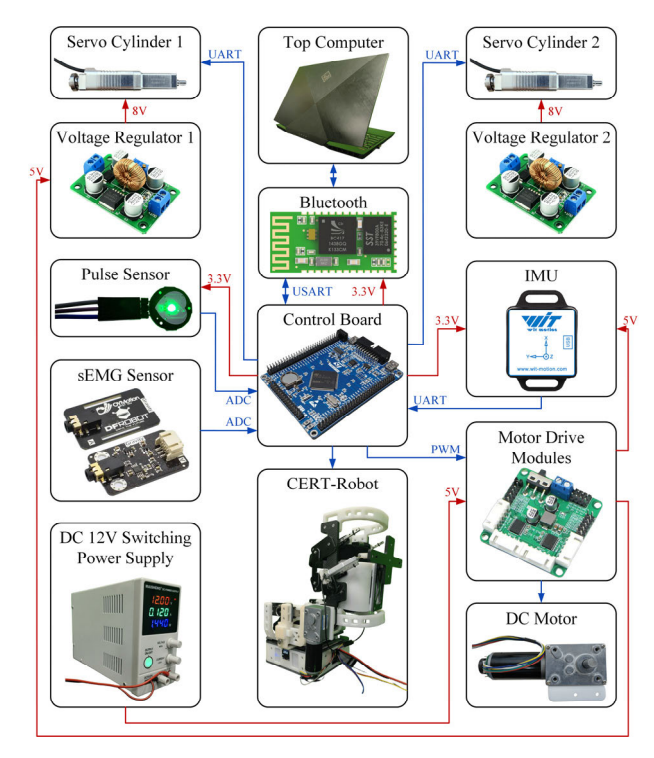


Fig. 4. Control system hardware architecture.

silicone pads bridge gaps between the exoskeleton and patient's arm.

C. Electrical Hardware and Sensor Unit

The system employs a hierarchical control architecture, comprising an upper computer (Qt platform with MATLAB neural network integration) and a lower computer (STM32F103ZET6 microcontroller), as shown in Fig. 4. The elbow joint rotation is driven by a 12V DC brushed motor (5840-31ZY, Xinyongtai, China) with 70 kg·cm rated torque, coupled with an incremental Hall encoder (JGB37-31ZY, Xinyongtai, China) for speed and position control. Traction motion is provided by a servo cylinder (LAF16-024D, Instech Robotics, China) with integrated force sensor (100 Hz sampling). sEMG signals are acquired via an Analog EMG Sensor (DFRobot, China) at 1000 Hz for motion prediction. Physiological monitoring includes heart rate detected by a Pulse Sensor (100 Hz, Xinweilai, China) and arm motion detected by an Inertial Measurement Unit (IMU) (100 Hz, WT61PC, Witte Intelligence, China). Data transmission between computers is facilitated by Bluetooth module (HC-05, Zave, China). Power is supplied through a regulated digital switching power supply (MN-305C, Maisheng, China) with overload protection.

D. Upper Computer Software

To realize the integration of hardware communication, motion control and signal feedback, the upper computer software is developed. The software architecture is designed according to the rehabilitation control strategy (see Section III). The system first evaluates the patient's rehabilitation phase, then selects appropriate training modes and parameters through the Qt-based interface. Command frames

are transmitted to the lower computer via a dedicated communication protocol, enabling remote control and real-time monitoring.

E. Safety

To ensure safety during operation, the ERT-Robot control system incorporates multiple safety protocols, including soft limits for joint rotation speed, angle and traction displacement. In addition, it continuously monitors heart rate signals P_u , triggering a warning prompt when exceeding 100 BPM (normal resting rate: 60-100 BPM) [27]. If unacknowledged within 3 s, the system initiates emergency shutdown.

III. ROBOT CONTROL METHODS

Based on the clinical performance of different rehabilitation phases, three rehabilitation control methods are developed: reciprocating passive (RP) training, active range of motion (AROM) training, and muscle strength (MS) training, as shown in Fig. 5.

A. Full-Cycle Rehabilitation Control

1) RP Training: Early-phase rehabilitation requires passive training, involving physician-assisted limb rotation and humeral surface-perpendicular forearm traction to enhance joint mobility and reduce soft tissue stiffness.

To replicate this clinically, it is necessary to tailor the motion parameters, such as joint angles and traction displacements, to achieve personalized motion control. The maximum joint angles and traction displacement are determined using physician demonstration based on admittance control. Joint movement employs PID-controlled sinusoidal trajectories between measured maximum flexion and extension angles, monitored via IMU-based closed-loop control. Simultaneously, the traction cylinder executes sinusoidal trajectories (0 mm to maximum displacement) under servo control, with 25 ms command intervals.

2) AROM Training: While passive training enhances joint mobility, robot-assisted passive training alone proves insufficient for functional recovery. Rehabilitation efficacy primarily depends on training intensity and patient engagement, rather than robotic assistance alone. To promote active participation, AROM training during mid-phase rehabilitation should be implemented.

The AROM model incorporates the patient's current strength level, utilizing deep learning to establish sEMG-joint angle-traction force correlations. sEMG data, processed by the lower computer, is transmitted via Bluetooth to the Qt platform for MATLAB-based neural network prediction of joint angles and traction displacements.

3) MS Training: This mode considers the patient's current strength level and extreme range of motion. During late-phase rehabilitation, following AROM training, patients demonstrate partial muscle recovery. The system applies controlled resistance during the joint flexion/extension to enhance muscle strength.

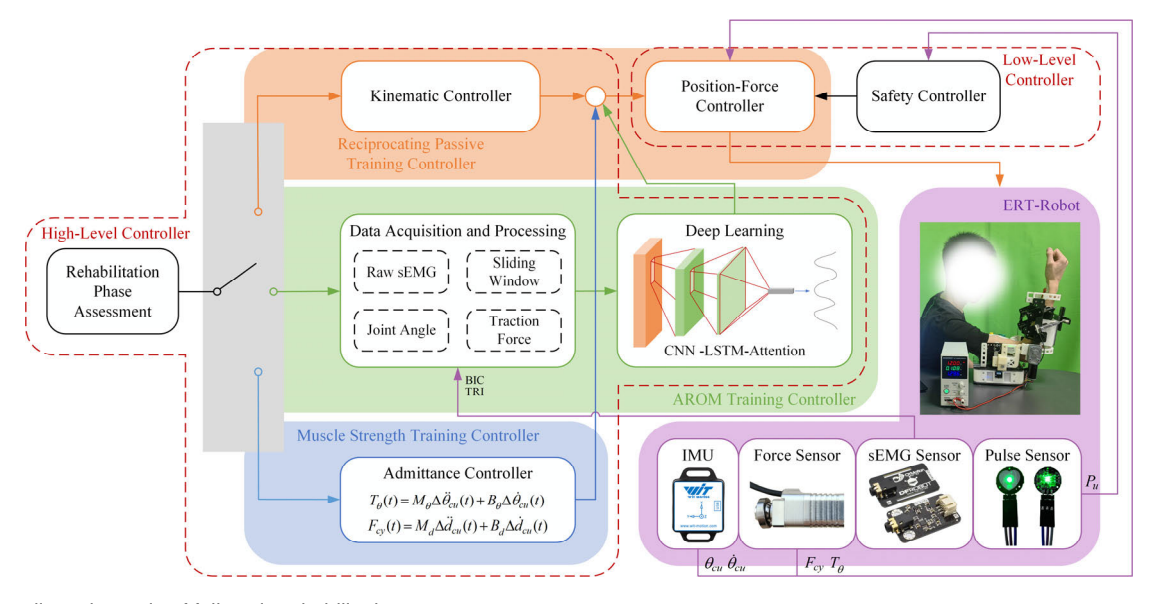


Fig. 5. Controller schematic of full-cycle rehabilitation strategy.

The admittance control model of the motor and the electric cylinder are expressed as

$$T_{\theta}(t) = M_{\theta} \Delta \ddot{\theta}_{cu}(t) + B_{\theta} \Delta \dot{\theta}_{cu}(t) \tag{1}$$

$$F_{cv}(t) = M_d \Delta \ddot{d}_{cu}(t) + B_d \Delta \dot{d}_{cu}(t) \tag{2}$$

where $T_{\theta}(t)$ and $F_{cy}(t)$ denote the joint torque on the motor and force on the electric cylinder exerted by the elbow joint, respectively. $\Delta \dot{\theta}_{cu}(t)$ and $\Delta \ddot{\theta}_{cu}(t)$ represent the angular velocity correction and angular acceleration correction of the desired and reference values, respectively. $\Delta \dot{d}_{cu}(t)$ and $\Delta \ddot{d}_{cu}(t)$ are the velocity correction and acceleration correction of the desired and reference values, respectively. M_{θ} and M_{d} are the inertia coefficients, B_{θ} and B_{d} are the damping coefficients. Through comprehensive MATLAB-based simulations of the DC motor and servo cylinder systems, the values of $M_{\theta}=20$, $B_{\theta}=100$, $M_{d}=200$ and $B_{d}=3000$ were determined.

B. Continuous Estimation of Joint Angles and Traction Forces Based on sEMG

1) Data Collection and Preprocessing: Six healthy subjects with no history of elbow disease participated in this study, including 3 males, aged 22.5 ± 0.5 years, height 176.5 ± 3.5 cm, weight 68.25 ± 3.25 kg, and 3 females, aged 23.0 ± 1.0 years, height 162.0 ± 3.0 cm, weight 51.75 ± 3.75 kg. All subjects were informed of the entire experimental procedure and signed an informed consent form. All experiments involving human subjects were approved by the Ethics Committee of Tianjin University.

The experimental setup is shown in Fig. 1 (d). Two muscles that are closely related to elbow joint movement are considered, including biceps brachii (BIC), triceps brachii (TRI). Prior to testing, subjects relaxed their upper limbs while the skin was cleansed with alcohol wipes to reduce impedance. Maximum voluntary contraction (MVC) data were recorded after signal processing. Subjects were secured to the robot using straps, with the system set to admittance

mode to facilitate human-robot interaction. Synchronous data acquisition of joint angles and traction forces was performed using IMUs and servo cylinder force sensors.

The anti-interference capability of the control system is of great significance [28], [29], [30]. To ensure the effective operation of the control system in the presence of noise and other disturbances, the sEMG signals are initially segmented into sliding windows comprising 300 sample points (approximately 3 s), with a sampling interval of 20 points (about 200 ms) between each window. A 50 Hz notch filter is employed to eliminate common power frequency interference, and a 20-500 Hz Butterworth bandpass filter is utilized to remove other potential interfering signals. After these filtering steps, the signals undergo full-wave rectification and linear enveloping to extract their features. Subsequently, normalization is conducted to ensure the stability and accuracy of the signals, as illustrated in Fig. 6. Additionally, considering the timer delays of approximately 20 ms in both the upper and lower computers, the overall delay of the control system is about 220 ms. MVC-based normalization eliminates inter-muscle variability. Signal smoothing is achieved through sliding square window processing

$$e_{sq}(i) = k \sum_{n=1}^{N} e_{filt}^{2}(i)$$
 (3)

where $e_{sq}(i)$ denotes the square value of sEMG, e_{filt} is the input value before processing, k represents the squaring factor, N is the window size, and I is the sampling point. Finally, the square root reduction is performed as follows to obtain the envelope signal $e_{env}(i)$

$$e_{env}(i) = \frac{1}{N} \sqrt{k e_{sq}(i)} \tag{4}$$

Four time-domain features are extracted from sEMG signals: mean absolute value (MAV), standard deviation (SD), root mean square (RMS), and wavelength. MAV and RMS

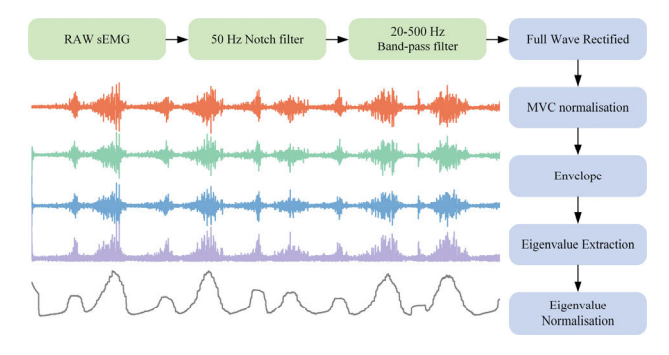


Fig. 6. sEMG preprocessing flow.

are commonly used to assess the intensity of muscle contraction and fatigue, while wavelength reflects signal complexity, indicating muscle contraction/relaxation states. SD enhances prediction accuracy.

The joint torque is derived from force sensor measurements, considering the fixed angular offset φ_{cy} between the sensor detection axis and forearm exoskeleton axis. Using the perpendicular distance x_{cy} (0.053m, obtained from 3D model measurements) between the force application point and motor shaft within their common plane, the torque is calculated as

$$T_{\theta}(t) = F_{cv}(t)x_{cv}\sin\varphi_{cv} \tag{5}$$

2) Deep Learning Based Neural Network Model: The input signals are feature extracts of the 2 muscles, which can be regarded as an image with the size of [300, 2]. A CNN-LSTM-Attention network is designed to solve estimation of elbow joint angles and traction forces. The proposed architecture employs a synergistic combination of: (a) CNN layers for spatial feature extraction from sliding window segments, (b) LSTM layers to capture temporal dependencies, and (c) an attention mechanism that dynamically weights salient signal phases to refine prediction accuracy.

As shown in Fig. 7, the network comprises two convolutional layers, one LSTM layer, two average pooling layers, and two fully connected layers, enabling continuous sEMGbased estimation. The sliding window images of the muscle activation are taken as the input and the corresponding elbow joint angle and traction force are taken as the output. Hyperparameters were optimized through a combination of grid search and cross-validation. CNN Layers: Kernel sizes (3×3) and stride lengths (1×1) were chosen to balance feature resolution and computational efficiency. LSTM Units: 128 units provided optimal trade-offs between model complexity and prediction latency. Attention Mechanism: A single-head attention layer was sufficient, as multi-head setups did not improve performance but increased inference time. Training Protocol: The model was trained using the Adam optimizer (learning rate = 0.001) with early stopping to prevent overfitting.

3) Evaluation Criteria: In order to quantitatively describe the regression ability of the model, three indices are adopted: mean absolute error (MAE) reflects estimation accuracy, root mean square error (RMSE) emphasizes larger deviations, and coefficient of determination (\mathbb{R}^2) evaluates overall fit. Optimal performance is indicated by MAE and RMSE approaching zero, and \mathbb{R}^2 approaching one.

IV. REHABILITATION FUNCTION EXPERIMENTS AND RESULTS

In Section III, the model was trained using data from six subjects. To verify the generalizability of the robotic system, an additional six new subjects were specifically recruited to participate in all experiments in this section. The data from these new subjects will be kept independent from the training dataset.

A. Functional Verification Experiments

- 1) Mechanism Range of Motion: In order to ascertain the mobility range of each mechanism of ERT-Robot, adjustments were made to the elbow joint angle, traction force angle, traction displacement and carrying angle under unloaded conditions, as shown in Fig. 8. The results show that the robot's mobility aligns with the human elbow joint range of -5° to 145° , traction force adjustment angle of 45° to 85° , and carrying angle range of -15° to 15° , all of which meet clinical rehabilitation needs.
- 2) Traction Function: The primary objective of design is to confirm the efficacy of traction exerted by the robot on the elbow joint. With the subject's arm maintained in a horizontal position, we measured the displacement of olecranon in both unassisted and reciprocating passive training scenarios. During this process, there is relative skin-to-bone movement on human arm. As the upper limb advances as a cohesive unit, the displacement of olecranon exhibits a specific relationship as

$$d_O = d_{td} + d_{sd} \tag{6}$$

where d_{td} denotes the traction displacement of the olecranon, and d_{sd} represents the sliding displacement of the skin on the arm relative to the underlying bone. The maximum value of d_O is compared across three situations for each subject: natural arm rotation, manual rehabilitation, and ERT-Robot-assisted rehabilitation. The olecranon's prominent anatomical position allows for clear identification without radiographic imaging, making it an ideal site for direct IMU placement. During elbow joint motion, the IMU accurately tracks three-dimensional olecranon displacement, with these kinematic measurements serving as the gold standard for quantifying traction displacement in our experimental protocol.

Six subjects were randomly numbered 1 to 6. The experimental data obtained from the two scenarios are shown in Fig. 9. $d_{O,NH}$ and $d_{O,NV}$ denote the horizontal and vertical displacements of olecranon in the natural state. Similarly, $d_{O,MH}$ and $d_{O,MV}$ are the horizontal and vertical displacements of ulnar olecranon during manual rehabilitation, while $d_{O,RH}$ and $d_{O,RV}$ represent the corresponding displacements during rehabilitation utilizing the ERT-Robot.

The experimental results, are shown in Fig. 10, indicate that, when compared to the natural arm rotation, the horizontal and vertical displacements of the olecranon were significantly increased using manual rehabilitation and robot-assisted rehabilitation. The difference between manual rehabilitation and robot-assisted rehabilitation is very small, with average differences in horizontal and vertical displacements were approximately 1.33% and 7.78%, respectively. As a

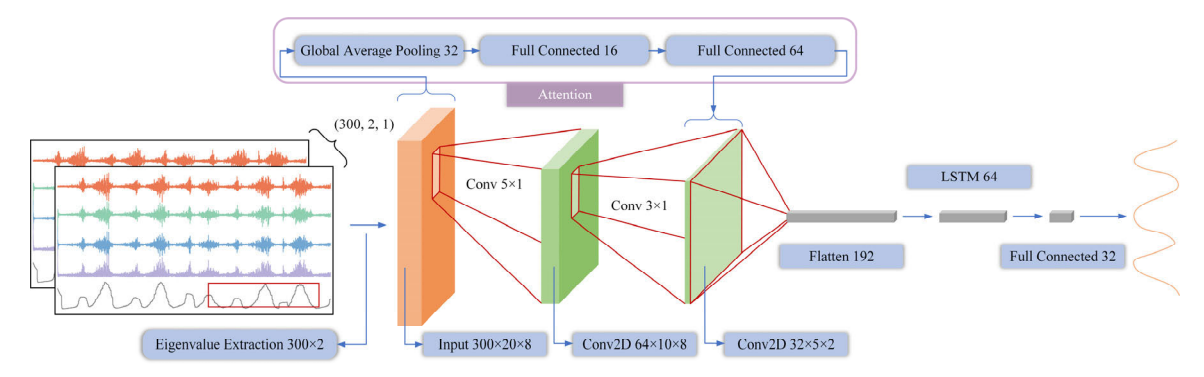


Fig. 7. Deep learning network architecture.

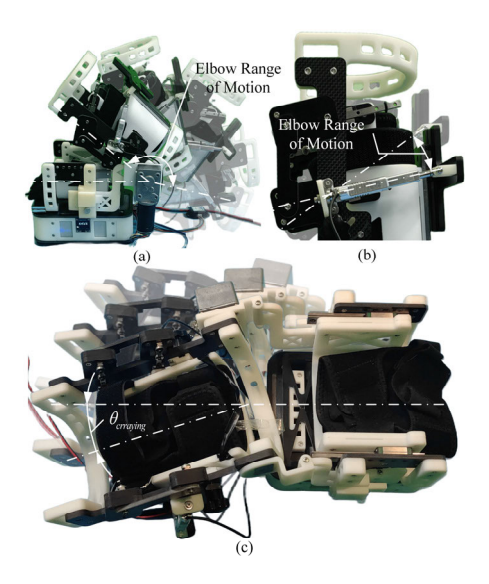


Fig. 8. ERT-Robot range of motion. (a) Elbow range of motion, (b) Adjustment range of traction angle, and (c) Adaptation range of carrying angle.

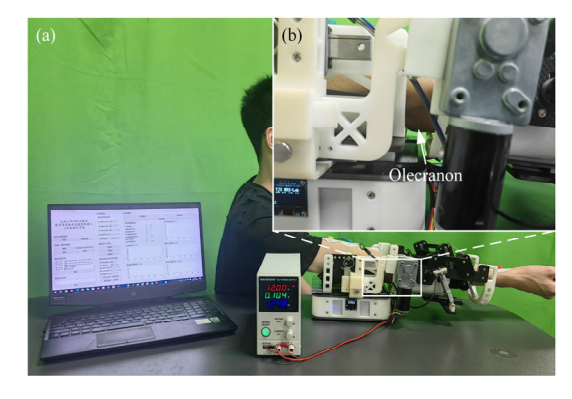


Fig. 9. Experimental setup. (a) Experimental scenario, (b) Position of the olecranon.

result, the effectiveness of the robotic traction function is validated.

3) Safety: Mutation simulation was performed on the heart rate signal, where the initial 20s is the normal heart rate signal of subject 1. At the 20th second, the signal was mutated to 110 BPM, exceeding the predefined heart rate threshold. The experimental results are shown in Fig. 11. Based on these results, the robot's emergency stop exhibited errors of 0.49° and 0.032 mm on the joint angle and traction

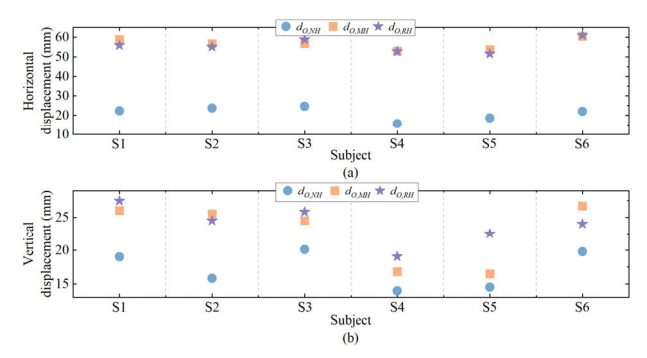


Fig. 10. Experimental results of the traction function. (a) Horizontal displacements of the olecranon in different subjects, (b) Vertical displacements of the olecranon in different subjects.

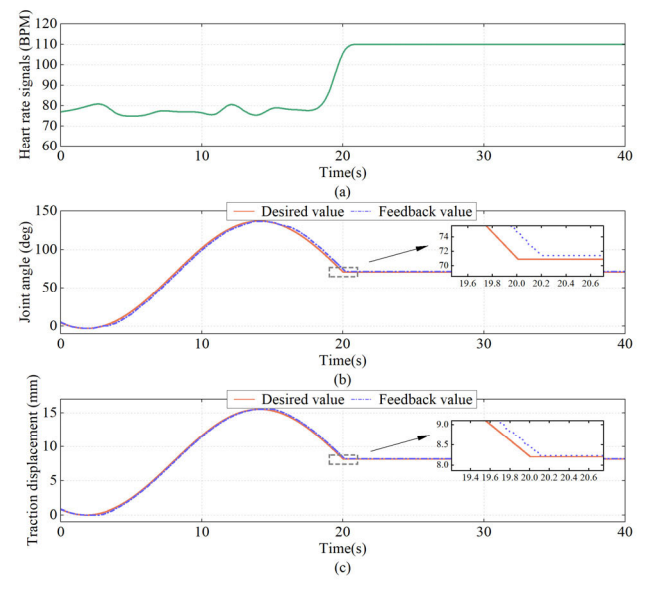


Fig. 11. Experimental results of emergency stop for subject 1. (a) Mutation simulation on the heart rate signal, (b) Desired and feedback joint angles, and (c) Desired and feedback traction displacements.

displacement. The corresponding response times are 175 ms and 133 ms on the motor and electric cylinder, both of which meet the requirements for a safe emergency stop of the robot.

B. Offline Estimation of Joint Angle and Traction Force

Comprehensive performance evaluations were conducted using conventional Backpropagation Neural Network (BPNN),

9.57

4 46

3.38

0.76

0.86

0.93

 \mathbb{R}^2

0.74

0.84

0.72

0.90

S3 - TF(N)

RM

SE

7.55

6.58

6.93

4.66

MA

8.34

7.68

5.09

Index S1 - JA (deg) S1 - TF(N)- JA (deg) - TF (N) S3 - JA (deg) S2 MA RMS MA RMS RM RMRM \mathbb{R}^2 \mathbb{R}^2 \mathbb{R}^2 \mathbb{R}^2 \mathbb{R}^2 SE SE SE E BPNN 0.70 5.65 6.62 0.75 3.65 3.55 0.86 6.84 4.48 0.728.78 5.38 8.35 8.68 0.73

4.64

8.34

3.30

5.35

5.21

4.49

TABLE I QUANTITATIVE EVALUATION OF THE OFFLINE ESTIMATION

0.80

0.79

0.91

8.44

7 32

5.68

8.66

6.46

3.64

0.76

0.82

0.91

9.68

7.16

7.34

11.3

7.88

0.75

0.83

0.93

4.88 3.12 Note: TPM-The proposed model, S-Subject, JA-Joint angle, TF-Traction force

8.89

LSTM

CNN

TPM

5.14

4 36

3.54

5.35

4.69

4.85

0.82

0.85

0.95

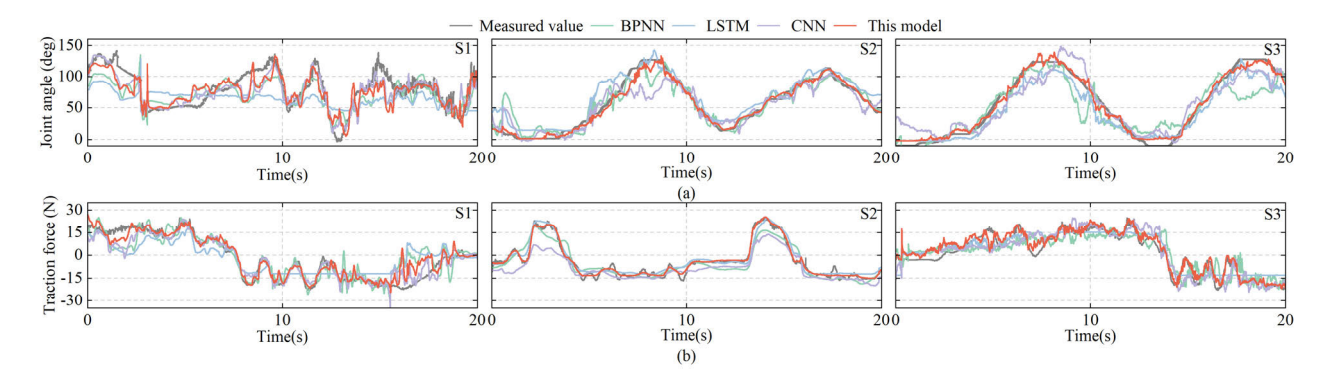
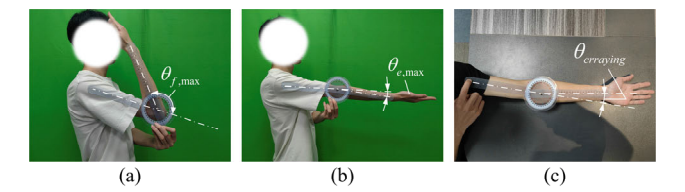


Fig. 12. Results of offline estimation for subject 1, subject 2, subject 3. (a) Estimation of joint angles, and (b) Estimation of traction forces.

LSTM, and CNN. Subjects were encouraged to control their muscles to realize motion intentions of flexion and extension. The sEMG sensor, IMU sensor, and force sensor were configured with sampling frequencies of 1000 Hz, 100 Hz, and 100 Hz, respectively. Each acquisition time is 20s. The experiments were replicated five times for each subject, with a 60s rest interval between set. Consequently, the sampling segment for each subject amounted to 20000. The number of sliding windows was calculated to be 986 ((20000-300+20)/20).

The offline estimation results of joint angle and traction force for each model are shown in Fig. 12. Evaluation results from a randomized trial for subject 1-3 are given. The quantitative evaluation results, shown in Table I, highlight the variations in model generalization capabilities. Table I comprehensively compares four neural network architectures (BPNN, CNN, LSTM, and CNN-LSTM-Attention) in predicting joint angles and traction forces, evaluating three key metrics: MAE, RMSE, and R². The CNN-LSTM-Attention hybrid model demonstrates statistically significant superiority across all metrics compared to standalone models. Specifically, the CNN-LSTM-Attention model exhibits a lower MAE value (p < 0.05), signifying a reduced average deviation between its predicted outcomes and the actual values. Its RMSE value is also lower (p < 0.05), indicating that the model generates smaller fluctuations in prediction errors, thereby yielding more stable results. Moreover, the model's higher R² value (p < 0.05) reflects a greater degree of alignment between its predicted results and the observed data. These findings substantiate the CNN-LSTM-Attention model's comprehensive superiority over other models in terms of prediction accuracy, error range, and stability. It is worth noting that the LSTM model demonstrated significantly lower estimation accuracy in Subject 1 compared to other methods, failing to achieve



Schematic diagram of measured joint angles. (a) Maximum Fig. 13. elbow flexion angle, (b) Maximum elbow extension angle, and (c) Carrying angle.

reliable estimation. This limitation stems from the algorithm's parameter sensitivity in elbow joint angle and traction force estimation, necessitating individual parameter calibration for each subject. This is challenging in practical applications, especially for patients with elbow fractures. In contrast, the CNN-LSTM-Attention model exhibited outstanding accuracy and stability across all quantitative indices.

C. Reciprocating Passive Training

To validate the effectiveness of the reciprocating passive training control strategy, the experiments focused on trajectory tracking accuracy during passive patient training were conducted.

A joint protractor was used to measure the subject's maximum elbow flexion angle $\theta_{f,max}$, maximum elbow extension $\theta_{e,\text{max}}$, carrying angle $\theta_{crraying}$, as shown in Fig. 13. The subject's joint angle control trajectory can be obtained as

$$\theta_d(t) = \frac{\theta_{f,\text{max}} - \theta_{e,\text{max}}}{2} \sin(kt + b) + \frac{\theta_{f,\text{max}} + \theta_{e,\text{max}}}{2}$$
 (7)

where $\theta_d(t)$ denotes the desired joint angle. k and b are constant coefficients.

The joint traction limit position was established through demonstration teaching. With the robot in admittance mode,

TABLE II
AVERAGE ERRORS FOR THREE EXPERIMENTS

Index		S1	S2	S3	S4	S5	S6	S1-6
RP	JA (deg)	2.46	2.74	3.10	3.55	2.67	3.71	3.04 ± 0.21
	TD (mm)	0.38	0.29	0.44	0.42	0.27	0.33	0.36 ± 0.004
AROM	JA (deg)	2.76	2.88	2.54	2.21	2.35	2.67	2.57 ± 0.05
	TF (N)	2.74	2.10	1.97	2.65	2.41	2.39	2.38 ± 0.08
MS	JA (deg)	1.63	1.74	1.38	1.44	1.45	1.60	1.54 ± 0.02
	TD (mm)	0.04	0.05	0.11	0.08	0.05	0.06	0.07 ± 0.0006

Note: S-Subject, JA-Joint angle, TD-Traction displacement, TF-Traction force

TABLE III
RMSE FOR THREE EXPERIMENTS

Index		S1	S2	S3	S4	S5	S6	S1-6
RP	JA (deg)	5.37	5.59	5.98	5.71	5.9	5.02	5.60± 0.11
	TD (mm)	1.27	1.04	1.17	0.91	1.13	0.87	1.07 ± 0.02
AROM	JA (deg)	6.02	6.46	5.47	8.14	5.7	5.14	6.16± 0.96
	TF (N)	7.29	7.5	7.74	5.8	6.47	6.69	6.92± 0.44
MS	JA (deg)	5.7	5.48	4.95	5.22	5.76	4.52	5.27± 0.19
	TD (mm)	0.19	0.15	0.17	0.16	0.16	0.17	0.17 ± 0.0001

Note: S-Subject, JA-Joint angle, TD-Traction displacement, TF-Traction force.

subjects performed ten elbow joint reciprocating movements. The average maximum cylinder position across these movements served as the passive training limit $d_{cy,\max}$. Thus, the individualized joint traction control trajectories can be expressed as

$$d_d(t) = \frac{d_{cy,\text{max}}}{2}\sin(kt+b) + \frac{d_{cy,\text{max}}}{2}$$
(8)

where $d_d(t)$ denotes the desired traction displacement.

Each subject completed the experiment six times, with only the data from one trial being displayed in the figures. The mean and variance of the errors are detailed in Tables II and III. The experimental results of the reciprocating passive training for subject 1 is shown in Fig. 14 and Fig. 15. The data of different subjects are shown in Tables II and III. The average error of the joint angle is $3.04^{\circ}\pm0.21^{\circ}$, accompanied by an average RMSE of $5.98^{\circ}\pm0.11^{\circ}$. Similarly, the average error of the traction displacement is $0.36 \text{ mm}\pm0.004 \text{ mm}$, with a corresponding average RMSE of $1.07 \text{ mm}\pm0.02 \text{ mm}$. These results indicate that the robot is capable of accurately tracking, confirming the robot's efficacy in reciprocating passive training.

D. Active Range of Motion Training

To verify the effectiveness of the AROM training control strategy, subjects were equipped with EMG sensors on both biceps and triceps brachii muscles. Following a 3-second signal acquisition period, subjects initiated autonomous elbow

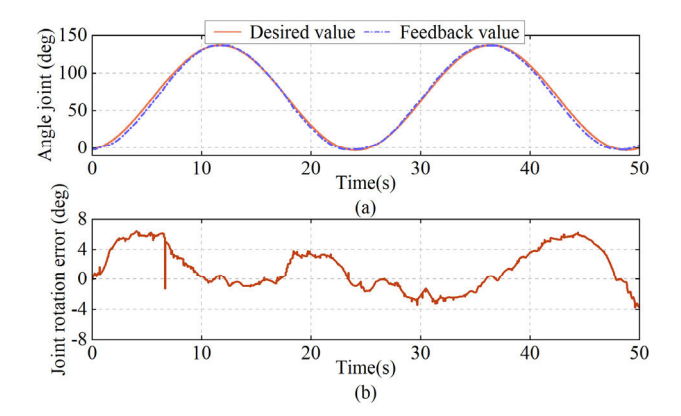


Fig. 14. Reciprocating passive training results: joint rotation angles for subject 1. (a) Desired and feedback joint rotation angles, and (b) Joint rotation errors.

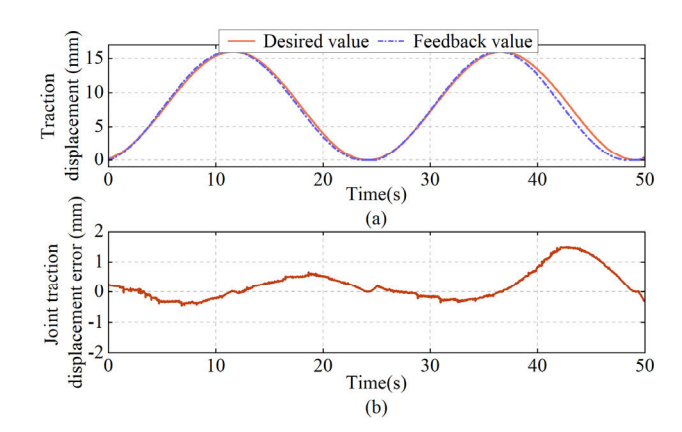


Fig. 15. Reciprocating passive training results: joint traction displacements for subject 1. (a) Desired and feedback joint traction displacements, and (b) Joint traction displacement errors.

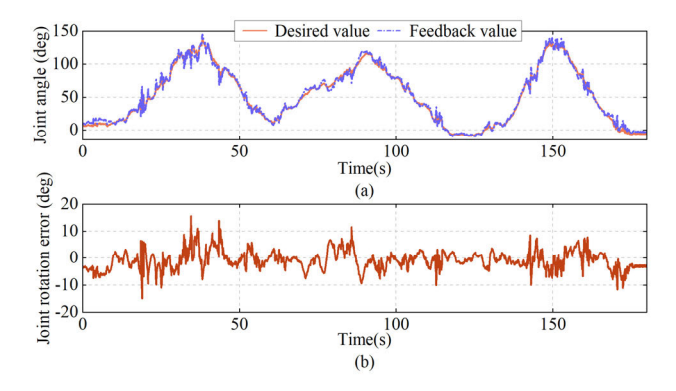


Fig. 16. AROM training results: joint rotation angles for subject 1. (a) Predicted and feedback joint rotation angles, and (b) Joint rotation errors.

rotation while the system predicted joint angles and traction forces at 200 ms intervals. The prediction and tracking performance for subject 1 are shown in Fig. 16 and Fig. 17. The data of different subjects on AROM training are shown in Tables II and III.

Experimental results demonstrate that the average error of the joint angle across different subjects in this training is $2.57^{\circ}\pm0.05^{\circ}$, with an average RMSE of $6.16^{\circ}\pm0.96^{\circ}$. Similarly, the traction force average error is $2.38 \text{ N}\pm0.08 \text{ N}$,

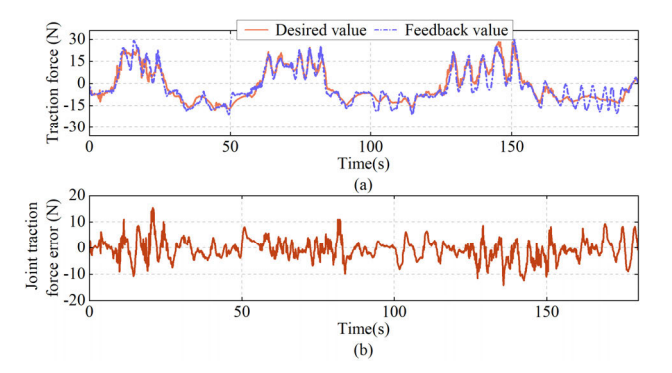


Fig. 17. AROM training results: joint traction displacements for subject 1. (a) Predicted and feedback joint traction forces, and (b) Joint traction force errors.

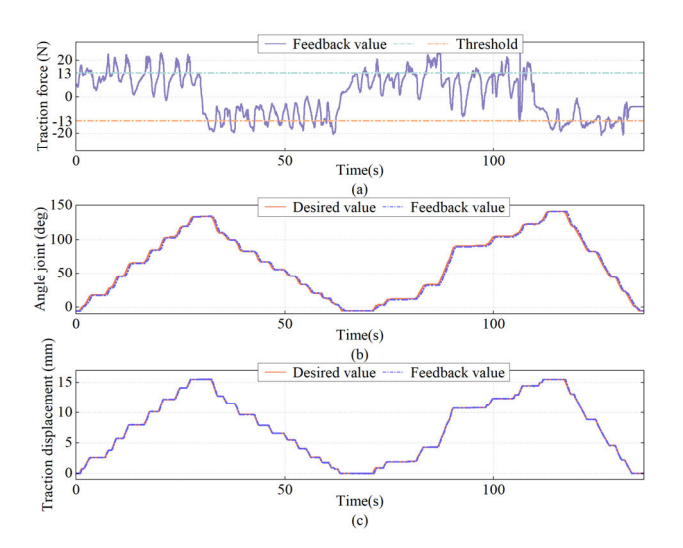


Fig. 18. MS training results for subject 1. (a) Desired and feedback joint traction forces, (b) Desired and feedback joint rotation angles, and (c) Desired and feedback joint traction displacements.

accompanied by an average RMSE of $6.92~\mathrm{N}\pm0.44~\mathrm{N}$. The experimental results show that the robot can accurately predict the movement intention of the limb and effectively implement AROM training.

E. Muscle Strength Training

In order to validate the effectiveness of the muscle strength training control strategy, we employed an admittance mode to apply simulated loads during elbow joint movement. Following clinical consultation with rehabilitation specialists, a safety threshold of 13 N was established for elbow traction forces across all six subjects. Force sensor data were recorded to determine the maximum moment, which served as the simulated load. The experimental results for subject 1 are shown in Fig. 18 and Fig. 19. The data of all subjects on the MS training are shown in Tables II and III.

Experimental results demonstrate that the average error of the joint angle across different subjects in the MS training is $1.54^{\circ}\pm0.02^{\circ}$ and the average error of the traction displacement is 0.07 mm ±0.0006 mm. Meanwhile, the average RMSE of the joint angle across subjects is $5.27^{\circ}\pm0.19^{\circ}$, and the average RMSE of the traction displacement is 0.17 mm ±0.0001 mm.

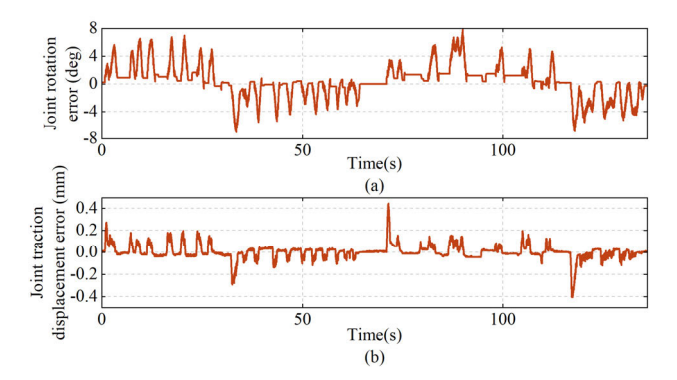


Fig. 19. MS training results: errors for subject 1. (a) Joint rotation errors, and (b) Joint traction displacement errors.

In addition, force signal analysis for subject 1 (see Fig. 18(a)) revealed stable load maintenance during elbow joint reciprocating movement, confirming the efficacy of the robot in muscle strength training.

V. DISCUSSION

This study presents a novel rehabilitation robotic system integrating elbow joint rotation and traction functions. The system features an innovative rotation mechanism accommodating upper limb carrying angles and an adjustable traction mechanism for soft tissue stretching, with customizable traction displacement and angle. Unlike previous robotic systems [10], [31], [32] that lacked joint traction or neglecting carrying angles [33], potentially leading to secondary injuries, the proposed ERT-Robot addresses these limitations through its comprehensive design. Furthermore, it overcomes the restricted motion range issues of [34] and [35], offering superior rehabilitation potential.

We propose a full-cycle rehabilitation control strategy incorporating joint traction adjustment across all rehabilitation phases, featuring three training modes: reciprocating passive training, AROM training, and muscle strength training. Experimental results demonstrate exceptional performance, with maximum joint angle RMSE of 8.14° for reciprocating passive and muscle strength training, and deep learning-based joint angle estimation achieving $R^2 = 0.958$ with RMSE = 4.85°. These results surpass comparable studies, such as the CNN-LSTM-Self-attention with Kalman filter by Zhang et al. [36] $(R^2 = 0.7)$, and the sEMG/IMU based predictions by Silva-Acosta et al. [37] (RMSE: 8.67° and 8.59°, respectively). In addition, while numerous studies have investigated elbow joint kinematics [38], [39], [40], the proposed ERT-Robot represents a significant advancement through its integrated control of joint traction force and displacement.

The proposed ERT-Robot addresses critical limitations in current elbow rehabilitation robot research, specifically the absence of joint traction function and comprehensive post-fracture rehabilitation control strategies. The developed traction mechanism, carrying angle adaptation, and full-cycle rehabilitation method demonstrate significant translational potential for other joints, particularly the knee, which shares similar physiological characteristics and rehabilitation principles with the elbow.

For fracture rehabilitation, elbow joint traction is crucial to prevent ligament adhesion and promote recovery of muscles, ligaments, and other soft tissues. This process requires precise control of both traction displacement and force to prevent secondary fractures. In neurological rehabilitation, however, joint traction is unnecessary since patients' skeletal systems and soft tissues remain intact, with only neural pathways affected. These distinct requirements demonstrate that the ERT-Robot is not only specifically designed for fracture rehabilitation but also fully adaptable to neurological rehabilitation scenarios.

While this study successfully demonstrates prototype functionality through healthy subject trials, there are still some limitations that need future investigation. The primary limitation of this study is its relatively small sample size, consisting exclusively of six healthy participants. To enhance the clinical relevance and generalizability of our findings, future work will recruit real clinical cases, expand the sample size, and include participants with varying ages, genders, and health conditions, particularly elbow fracture patients. Secondly, the sEMG-based motion estimation algorithm, currently employing empirically determined parameters, requires further refinement to enhance its predictive accuracy and adaptability. Finally, the current experiments primarily focus on the short-term traction performance and rehabilitation training outcomes. Future work will focus on conducting long-term follow-up assessments to evaluate the sustainability of joint function recovery and long-term muscle strength improvement, further validating the clinical application value of the ERT-Robot. To comprehensively evaluate the ERT-Robot's clinical efficacy, we will also incorporate standardized clinical evaluation indicators, including Activities of Daily Living scores and Mayo Elbow Performance scores.

VI. CONCLUSION

In this paper, a novel robotic system integrating elbow rotation and traction for full-cycle postoperative rehabilitation is developed. The mechanical design incorporates: (1) a rotation mechanism accommodating upper limb carrying angles, and (2) an adaptive traction mechanism with adjustable displacement and angle, capable of accommodating diverse patient anthropometrics for effective soft tissue stretching. A full-cycle rehabilitation control strategy encompassing three rehabilitation modes, that is reciprocating passive training, AROM training, and muscle strength training, is implemented. The hierarchical control architecture combines a lower-level PID controller for position and force regulation with an upper-level CNN-LSTM-Attention network for sEMG-based estimation of joint angles and traction forces. The experiments with six healthy subjects validated the feasibility and effectiveness of the proposed robotic system in robot-assisted elbow rehabilitation. This study provides a technical reference for robotic-assisted rehabilitation after elbow fracture surgery and has potential clinical applicability.

REFERENCES

[1] A.-M. Wu et al., "Global, regional, and national burden of bone fractures in 204 countries and territories, 1990–2019: A systematic analysis from the global burden of disease study 2019," *Lancet Healthy Longev*, vol. 2, pp. E580–E592, Sep. 2021, doi: 10.1016/S2666-7568(21)00172-0.

- [2] M. A. Padilla-Castaneda et al., "A virtual reality system for robotic-assisted orthopedic rehabilitation of forearm and elbow fractures," in *Proc. IEEE Int. Conf. Intell. Rob. Syst.*, May 2013, pp. 1506–1511, doi: 10.1109/IROS.2013.6696548.
- [3] J. D. A. Divierte et al., "A review on elbow biomechanics and medical applications in the field of biomedical engineering," in Proc. IEEE Int. Conf. Humanoid, Nanotechnol., Inf. Technol., Commun. Control, Environ., Manag. (HNICEM), Dec. 2022, pp. 1–6, doi: 10.1109/HNICEM57413.2022.10109481.
- [4] K. Cisek and J. D. Kelleher, "Current topics in technology-enabled stroke rehabilitation and reintegration: A scoping review and content analysis," *IEEE Trans. Neural Syst. Rehabil. Eng.*, vol. 31, pp. 3341–3352, 2023, doi: 10.1109/TNSRE.2023. 3304758.
- [5] Z. Lovrenovic and M. Doumit, "Development and testing of a passive walking assist exoskeleton," *Biocybernetics Biomed. Eng.*, vol. 39, no. 4, pp. 992–1004, Oct. 2019.
- [6] Y. Ji, X. Lang, B. Wu, Y. Fan, Q. Zheng, and X. Yang, "Conceptual design and preliminary experiment of an orthopedic rehabilitation exoskeleton based on the coupled movable pulley mechanism (CMPM)," in *Proc. World Rehabil. Robot Conv. (WRRC)*, Aug. 2024, pp. 1–6, doi: 10.1109/WRRC62201.2024.10696897.
- [7] M. Ni, J. Liu, Z. He, and T. Sun, "A sEMG-based active-passive fusion rehabilitation method for ankle fracture rehabilitation robot after surgery," *IEEE Robot. Autom. Lett.*, vol. 10, no. 3, pp. 2894–2901, Mar. 2025, doi: 10.1109/LRA.2025.3531715.
- [8] J. C. Perry, J. Rosen, and S. Burns, "Upper-limb powered exoskeleton design," *IEEE/ASME Trans. Mechatronics*, vol. 12, no. 4, pp. 408–417, Aug. 2007, doi: 10.1109/TMECH.2007.901934.
- [9] T. Chen, R. Casas, and P. S. Lum, "An elbow exoskeleton for upper limb rehabilitation with series elastic actuator and cable-driven differential," *IEEE Trans. Robot.*, vol. 35, no. 6, pp. 1464–1474, Dec. 2019, doi: 10.1109/TRO.2019.2930915.
- [10] M. Irshaidat, M. Soufian, A. Al-Ibadi, and S. Nefti-Meziani, "A novel elbow pneumatic muscle actuator for exoskeleton arm in post-stroke rehabilitation," in *Proc. 2nd IEEE Int. Conf. Soft Robot. (RoboSoft)*, Apr. 2019, pp. 630–635, doi: 10.1109/ROBOSOFT.2019.8722813.
- [11] T. Wilps, R. A. Kaufmann, S. Yamakawa, and J. R. Fowler, "Elbow biomechanics: Bony and dynamic stabilizers," *J. Hand Surg.*, vol. 45, no. 6, pp. 528–535, Apr. 2020, doi: 10.1016/j.jhsa.2020.01.016.
- [12] JAS. (May 2024). JAS SPS Elbow. [Online]. Available: https://www.jointactivesystems.com/products/jas-sps-elbow
- [13] JAS. (May 2024). JAS GL Elbow. [Online]. Available: https://www. jointactivesystems.com/products/jas-gl-elbow
- [14] R. Raj, R. Ramakrishna, and K. S. Sivanandan, "A real time surface electromyography signal driven prosthetic hand model using PID controlled DC motor," *Biomed. Eng. Lett.*, vol. 6, no. 4, pp. 276–286, Nov. 2016, doi: 10.1007/S13534-016-0240-4.
- [15] Q. Wu, B. Chen, and H. Wu, "RBFN-based adaptive backstepping sliding mode control of an upper-limb exoskeleton with dynamic uncertainties," *IEEE Access*, vol. 7, pp. 134635–134646, 2019, doi: 10.1109/ACCESS.2019.2941973.
- [16] B. Brahmi, M. Saad, C. Ochoa-Luna, M. H. Rahman, and A. Brahmi, "Adaptive tracking control of an exoskeleton robot with uncertain dynamics based on estimated time-delay control," *IEEE/ASME Trans. Mechatronics*, vol. 23, no. 2, pp. 575–585, Apr. 2018, doi: 10.1109/TMECH.2018.2808235.5.
- [17] A. Riani, T. Madani, A. Benallegue, and K. Djouani, "Adaptive integral terminal sliding mode control for upper-limb rehabilitation exoskeleton," *Control Eng. Pract.*, vol. 75, pp. 108–117, Jun. 2018, doi: 10.1016/j.conengprac.2018.02.013.
- [18] Q. Wu and Y. Chen, "Development of an intention-based adaptive neural cooperative control strategy for upper-limb robotic rehabilitation," *IEEE Robot. Autom. Lett.*, vol. 6, no. 2, pp. 335–342, Apr. 2021, doi: 10.1109/LRA.2020.3043197.
- [19] F. S. di Luzio et al., "Bio-cooperative approach for the humanin-the-loop control of an end-effector rehabilitation robot," *Frontiers Neurorobot.*, vol. 12, p. 67, Oct. 2018, doi: 10.3389/fnbot.2018.00067.
- [20] N. Vitiello et al., "NEUROExos: A powered elbow exoskeleton for physical rehabilitation," *IEEE Trans. Robot.*, vol. 29, no. 1, pp. 220–235, Feb. 2013, doi: 10.1109/TRO.2012.2211492.
- [21] S. Dalla Gasperina et al., "AGREE: A compliant-controlled upper-limb exoskeleton for physical rehabilitation of neurological patients," *IEEE Trans. Med. Robot. Bionics*, vol. 5, no. 1, pp. 143–154, Feb. 2023, doi: 10.1109/TMRB.2023.3239888.

- [22] A. A. Blank, J. A. French, A. U. Pehlivan, and M. K. O'Malley, "Current trends in robot-assisted upper-limb stroke rehabilitation: Promoting patient engagement in therapy," *Current Phys. Med. Rehabil. Rep.*, vol. 2, no. 3, pp. 184–195, Sep. 2014, doi: 10.1007/s40141-014-0056-z.
- [23] Q. Wu, Z. Wang, and Y. Chen, "SEMG-based adaptive cooperative multi-mode control of a soft elbow exoskeleton using neural network compensation," *IEEE Trans. Neural Syst. Rehabil. Eng.*, vol. 31, pp. 3384–3396, 2023, doi: 10.1109/TNSRE.2023.3306201.
- [24] K. Gui, H. Liu, and D. Zhang, "A practical and adaptive method to achieve EMG-based torque estimation for a robotic exoskeleton," *IEEE/ASME Trans. Mechatronics*, vol. 24, no. 2, pp. 483–494, Apr. 2019, doi: 10.1109/TMECH.2019.2893055.
- [25] G. Paraskevas, A. Papadopoulos, B. Papaziogas, S. Spanidou, H. Argiriadou, and J. Gigis, "Study of the carrying angle of the human elbow joint in full extension: A morphometric analysis," Surgical Radiologic Anatomy, vol. 26, no. 1, pp. 19–23, Feb. 2003, doi: 10.1007/s00276-003-0185-z.
- [26] Information and Documentation Chinese Adult Body Size, document GB/T 10002023, Nat. Standardization Tech. Committee, Beijing, China, 2024.
- [27] L. M. Westergaard et al., "Ventricular rate in atrial fibrillation and the risk of heart failure and death," *Europace*, vol. 25, no. 5, pp. 1–9, May 2023, doi: 10.1093/europace/euad088.
- [28] C. Wang, L. Peng, and Z.-G. Hou, "A control framework for adaptation of training task and robotic assistance for promoting motor learning with an upper limb rehabilitation robot," *IEEE Trans. Syst., Man, Cybern., Syst.*, vol. 52, no. 12, pp. 7737–7747, Dec. 2022, doi: 10.1109/TSMC.2022.3163916.
- [29] J. Xu, K. Huang, T. Zhang, M. Zhao, A. Ji, and Y. Li, "Mirror adaptive impedance control of multi-mode soft exoskeleton with reinforcement learning," *IEEE Trans. Autom. Sci. Eng.*, vol. 22, pp. 6773–6785, 2025, doi: 10.1109/TASE.2024.3454444.
- [30] J. Xu, L. Xu, A. Ji, Y. Li, and K. Cao, "A DMP-based motion generation scheme for robotic mirror therapy," *IEEE/ASME Trans. Mechatronics*, vol. 28, no. 6, pp. 3120–3131, Dec. 2023, doi: 10.1109/TMECH.2023.3255218.
- [31] J. Zhang, C. Xu, Z. Fang, X. Sun, and W. Chen, "Design of an underactuated body fixture for a 7-DOF cable-driven upper limb exoskeleton," in *Proc. 15th IEEE Conf. Ind. Electron. Appl. (ICIEA)*, Nov. 2020, pp. 1538–1543.

- [32] J. Jeong et al., "Soft wearable robot with shape memory alloy (SMA)-based artificial muscle for assisting with elbow flexion and forearm supination/pronation," *IEEE Robot. Autom. Lett.*, vol. 7, no. 3, pp. 6028–6035, Jul. 2022, doi: 10.1109/LRA.2022. 3161700.
- [33] W. Qian et al., "CURER: A lightweight cable-driven compliant upper limb rehabilitation exoskeleton robot," *IEEE/ASME Trans. Mechatronics*, vol. 28, no. 3, pp. 1730–1741, Jun. 2023, doi: 10.1109/TMECH.2022.
- [34] A. U. Pehlivan, O. Celik, and M. K. O'Malley, "Mechanical design of a distal arm exoskeleton for stroke and spinal cord injury rehabilitation," in *Proc. IEEE Int. Conf. Rehabil. Robot.*, Jun. 2011, pp. 1–5, doi: 10.1109/ICORR.2011.5975428.
- [35] Z. Yang and S. Guo, "A hybrid motion stiffness control of variable stiffness actuator for upper limb elbow joints rehabilitation," in *Proc. IEEE Int. Conf. Mechatronics Autom. (ICMA)*, Aug. 2022, pp. 1324–1328, doi: 10.1109/ICMA54519.2022.9855934.
- [36] A. Zhang, Q. Li, Z. Li, and J. Li, "Upper limb movement decoding scheme based on surface electromyography using attentionbased Kalman filter scheme," *IEEE Trans. Neural Syst. Rehabil. Eng.*, vol. 31, pp. 1878–1887, 2023, doi: 10.1109/TNSRE.2023. 3262269.
- [37] V. D. C. Silva-Acosta, I. Román-Godínez, S. Torres-Ramos, and R. A. Salido-Ruiz, "Automatic estimation of continuous elbow flexion-extension movement based on electromyographic and electroencephalographic signals," *Biomed. Signal Process. Control*, vol. 70, Sep. 2021, Art. no. 102950, doi: 10.1016/j.bspc.2021. 102950.
- [38] Y. Chen, X. Zhao, and J. Han, "Hierarchical projection regression for online estimation of elbow joint angle using EMG signals," *Neural Comput. Appl.*, vol. 23, nos. 3–4, pp. 1129–1138, Jul. 2012, doi: 10.1007/s00521-012-1045-8.
- [39] L. Peng, Z.-G. Hou, and W. Wang, "A dynamic EMG-torque model of elbow based on neural networks," in *Proc. 37th Annu. Int. Conf. IEEE Eng. Med. Biol. Soc. (EMBC)*, Aug. 2015, pp. 2852–2855, doi: 10.1109/EMBC.2015.7318986.
- [40] S. Guo, Z. Yang, and Y. Liu, "EMG-based continuous prediction of the upper limb elbow joint angle using GRNN," in *Proc. IEEE Int. Conf. Mechatronics Autom. (ICMA)*, Aug. 2019, pp. 2168–2173, doi: 10.1109/ICMA.2019.8816401.